

LARGE-EDDY SIMULATION OF A HYPERSONIC TURBULENT BOUNDARY LAYER OVER A CONE IN SUPPORT OF FOCUSED LASER DIFFERENTIAL INTERFEROMETRY (FLDI) MEASUREMENTS

Takahiko Toki

School of Mechanical Engineering
Purdue University
West Lafayette, Indiana 47906, USA
ttoki@purdue.edu

Victor C. B. Sousa

School of Mechanical Engineering
Purdue University
West Lafayette, Indiana 47906, USA
vsousa@purdue.edu

Yongkai Chen

School of Mechanical Engineering
Purdue University
West Lafayette, Indiana 47906, USA
chen1305@purdue.edu

Giannino Ponchio Camillo

German Aerospace Center (DLR)
Institute of Aerodynamics and Flow Technology
Göttingen, Germany
giannino.ponchiocamillo@dlr.de

Alexander Wagner

German Aerospace Center (DLR)
Institute of Aerodynamics and Flow Technology
Göttingen, Germany
alexander.wagner@dlr.de

Carlo Scalo

School of Mechanical Engineering
Purdue University
West Lafayette, Indiana 47906, USA
scalo@purdue.edu

ABSTRACT

Large-eddy simulations (LES) of a hypersonic turbulent boundary layer over a cone are carried out to provide instantaneous data for future computational Focused Laser Differential Interferometry (cFLDI) calculations. First, a precursor Reynolds-Averaged Navier-Stokes (RANS) simulation is performed to provide mean-flow velocity and temperature profiles as inlet boundary condition for the LES. A rescaling method is used to achieve fully turbulent conditions as early as possible in the domain, resulting in an approximate recovery length of 5 cm. The LES simulations are based on a new Quasi-Spectral Viscosity (QSV) closure of the filtered Navier-Stokes equations Sousa & Scalo (2022a). Time series of local density fluctuations collected from two points taken 2 mm apart, mimicking typical FLDI measurements, show a strong correlation, with the data extracted downstream exhibiting the expected convective delay. Observation of instantaneous density fluctuations in wall-parallel planes reveals that the density field in the buffer layer has a streaky structure, with large streamwise coherence, which disappears further away from the wall. This results in a density power spectrum focused on lower frequencies near wall, with a broader energy distribution, including higher frequencies, in the outer layer. Future work will focus on simulating higher Reynolds numbers and performing cFLDI simulations on the LES data.

INTRODUCTION

The state of the boundary layer on high-speed flight vehicles is a paramount factor in their design and performance. The extreme conditions imposed by near-wall turbulence ren-

der the evaluation of such flow fields valuable.

Convection velocities of over 2 km/s are present in hypersonic boundary layers in atmospheric flight conditions. Furthermore, in a turbulent state, relevant energy levels cascade to flow field structures smaller than the boundary layer height, yielding frequencies in the order of MHz. This set of conditions motivates the need for time-resolved high-fidelity flow field simulation, and defines the requirements for flow diagnostic techniques.

Among the few techniques with such bandwidth for experimental evaluation of hypersonic turbulence is Focused Laser Differential Interferometry (FLDI), a focusing line-of-sight technique capable of fine temporal and spatial resolution in the vicinity of the center plane of the probing volume (Parziale *et al.*, 2012). The downside of this focusing ability is the added complexity to the interpretation of the data, stemming from a sensitive length, which is dependent on the size of the convecting disturbances in the flow field. This way, the conversion of FLDI values into flow field density quantities requires flow field information.

A promising approach to overcome this challenge is to make use of a computational equivalent of the experimental FLDI procedures, as demonstrated by Lawson & Austin (2021). An accurate simulation of FLDI measurements, referred to as computational FLDI, or cFLDI, is possible by applying a ray-tracing algorithm to high-fidelity, instantaneous three-dimensional flow data.

In this study, a high-fidelity large-eddy simulation is carried out to provide instantaneous data for future cFLDI studies, virtually applying the experimental setup described in Camillo & Wagner (2022) to a fully turbulent hypersonic boundary

Table 1. List of referred experimental flow conditions (Wagner, 2014).

Re_m [1/m]	4.1×10^6
p_∞ [Pa]	2129
T_∞ [K]	268
ρ_∞ [kg/m ³]	0.0276
u_∞ [m/s]	2422
M_∞	7.4

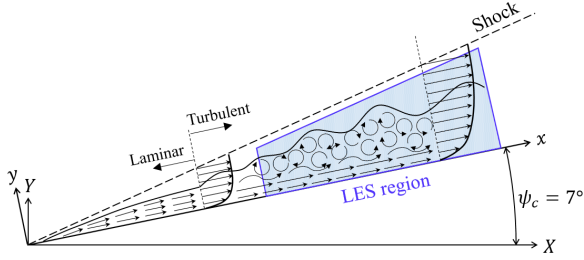


Figure 1. Sketch of the present hypersonic boundary layer configuration.

layer.

PROBLEM FORMULATION

Computational setup

The numerical study performed in this work is based on experiments conducted in the DLR High Enthalpy Shock Tunnel Göttingen, HEG (Wagner, 2014; Hannemann *et al.*, 2018). The present configuration is a hypersonic boundary layer over a 7 degree half angle cone, and test condition of $Re_m = 4.1 \times 10^6 \text{ m}^{-1}$ is chosen. The same flow was simulated by Sousa *et al.* (2019) but in an axisymmetric fashion only. In table 1, $Re_m \equiv \rho_\infty u_\infty / \mu_\infty$ is the Reynolds number per meter. The subscript ∞ indicates free stream conditions. In table 1, p is pressure, T is temperature, ρ is density, u is velocity, and M is Mach number. Figure 1 provides a sketch of the present configuration. In the experiment, a conical shock is attached to the tip of the cone and a boundary layer is formed on the cone surface under the shock. The laminar boundary layer starts from the tip and transition to turbulence happens further downstream on the surface. In this study, the turbulent region under the shock is simulated using a new LES technique called the Quasi-Spectral Viscosity (QSV) Large-Eddy Simulation, described in Sousa & Scalo (2022a).

To impose physical turbulent inlet boundary conditions in the QSV-LES, a preliminary axisymmetric Reynolds-Averaged Navier-Stokes (RANS) simulation is carried out. The inlet of the computational domain is located at $x = 0.045$ m from the cone tip, where x is a streamwise coordinate. The domain length in streamwise direction L_x is 1 m. The domain length in the wall-normal direction L_y is 0.0022 m at the inlet and 0.05 m at the outlet. These lengths are decided so that the upper domain is located under the shock. The azimuthal extension is 1.5 degrees. At the inlet and the upper boundary, a Dirichlet boundary conditions are imposed. The flow properties at the upper boundary are analytically derived

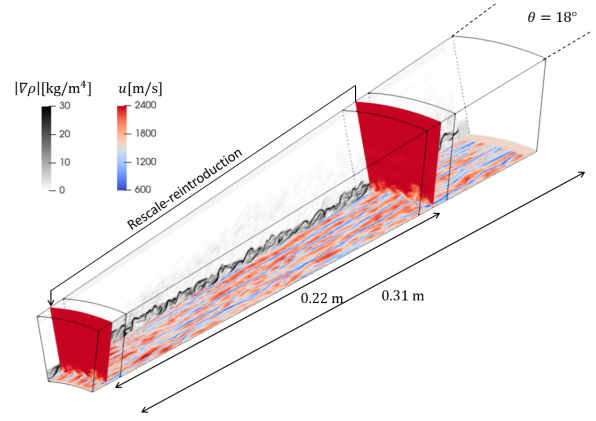


Figure 2. Schematic of the present QSV-LES of a hypersonic boundary layer over a cone. Contours in wall-parallel and cross-flow planes show streamwise velocity fields. A contour in a side plane shows magnitude of density gradient.

by the Taylor-Maccoll inviscid solution (Taylor & Maccoll, 1933), and those at the inlet are given by combining the Taylor-Maccoll inviscid solution with a viscous solution for the cone boundary layer (Lees, 1956). At the wall, an isothermal and no-slip boundary condition is imposed with the wall temperature of 300 K. At the outlet, a homogeneous Neumann condition is imposed for all flow quantities. In addition, sponge layers are used at the inlet, outlet, and upper boundaries. The length of the sponge layers at the inlet and outlet are 3% of the total computational domain extent in the streamwise direction. That at the upper boundary is 5% of the wall normal extent. The number of grid points are $N_x \times N_y \times N_\theta = 4096 \times 128 \times 6$. Spalart-Allmaras (SA) model (Spalart & Allmaras, 1992) is used as RANS model. To simulate a boundary layer with turbulent transition, a trip is located at $x = 0.3$ m. The trip location is decided based on the experiment by Wagner (2014).

Only a part of the RANS computational domain is simulated using QSV-LES. Figure 2 shows the domain length for the present QSV-LES, and figure 3 depicts the relative positioning between the present RANS and QSV-LES. The inlet of the QSV-LES domain is located at $x = 0.6$ m, and its domain length in streamwise direction L_x is 0.31 m. The azimuthal angle is extended to 18 degrees. The number of grid points are $N_x \times N_y \times N_\theta = 1280 \times 128 \times 112$. The measurement point of FLDI in the experiment is located at $x = 0.814$ m, and the computational domain for QSV-LES is designed to include the measurement point. To generate a realistic inflow turbulence at the inlet, the rescaling method is used (Urbin & Knight, 2001). The inlet profiles of mean quantities are given by the RANS results at $x = 0.6$ m. Turbulent fluctuations for $0.83 \leq x \leq 0.85$ are extracted, and the fluctuations are scaled and imposed upon the mean quantities for $0.6 \leq x \leq 0.62$. The distance between the recycling box and the inlet is 0.22 m. This length is equivalent to $51 \delta_{99}$ at $x = 0.6$ m, where δ_{99} is 99% of boundary layer thickness.

Numerical method

In the QSV-LES technique, Favre-filtered Navier-Stokes equations are solved via a six-order compact finite difference code originally developed by Nagarajan *et al.* (2003) and now under continued development at Purdue. The QSV approach by Sousa & Scalo (2022a) is used for turbulence closure, and the present QSV-LES is the first practical case where this approach is used. The approach was also developed to be appli-

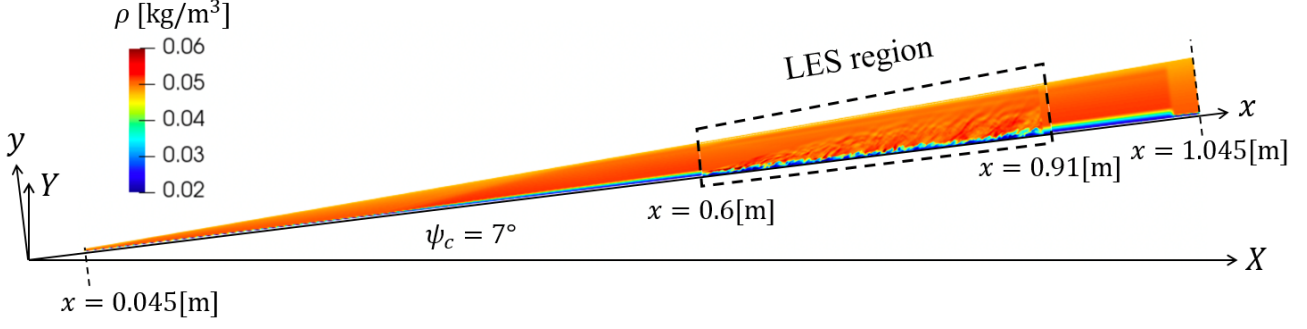


Figure 3. Positional relationship of computational domains between the present RANS and LES.

cable to unstructured grids (Sousa & Scalio, 2022b). The time integration is carried out by a four-stage third order strong stability preserving (SSP) Runge-Kutta scheme (Gottlieb, 2005). In order to ensure time stability, the conservative variables are filtered using sixth-order compact filter described by Lele (1992). Its filter coefficient is 0.495.

RESULTS

Flow statistics

Since the mean quantities at the inlet are given by the RANS results, a recovery process from the RANS profiles to the real turbulent boundary profiles should happen from the inlet. To confirm that a fully developed boundary layer is formed after the recovering process, flow statistics are examined.

Figure 4 compares wall heat flux profiles of the present RANS and LES with the experiment (Wagner, 2014). The wall heat fluxes are normalized by their laminar value at $x = 0.232$ m. The heat flux from the QSV-LES has a sharp peak around $x = 0.62$ m and thereafter a plateau develops for $0.65 \leq x \leq 0.85$. In the plateau region, the QSV-LES heat flux is comparable with the experimental one. The sharp peak around $x = 0.62$ m implies the recovering process happens around this region, and the plateau implies the real turbulent boundary profiles are formed after $x = 0.65$ m.

To investigate whether the flow field reaches the real turbulent profiles after $x = 0.65$ m, figure 5 shows mean profiles of velocity and temperature, and figure 6 depicts velocity fluctuation correlations. The mean profiles and fluctuation correlations are calculated by averaging in the azimuthal direction and time; $(\bar{\cdot})$ indicates Favre average; the notation $(\cdot)''$ indicates fluctuations about the Favre average. The velocity fluctuation correlations are computed as

$$u''_{rms} = \sqrt{\overline{u''u''}}, v''_{rms} = \sqrt{\overline{v''v''}}, w''_{rms} = \sqrt{\overline{w''w''}}. \quad (1)$$

The mean velocity is normalized by the boundary layer edge value, and the mean temperature is normalized by the wall value. Figure 5 also includes transformed velocity profiles by Trettel & Larsson (2016) transformation law. The velocity fluctuation correlations in figure 6 are normalized by the semi-local friction velocity $u_{\tau}^* \equiv \sqrt{\tau_w/\rho}$, where τ_w is wall fluid shear stress, and $(\bar{\cdot})$ indicates averaging in the azimuthal direction and time.

The mean velocity monotonically increases from the wall at any x -location, and all profiles collapse to each other. The mean temperature increases from the wall to $y/\delta_{99} \approx 0.05$ and further decreases to the far field. All temperature profiles also

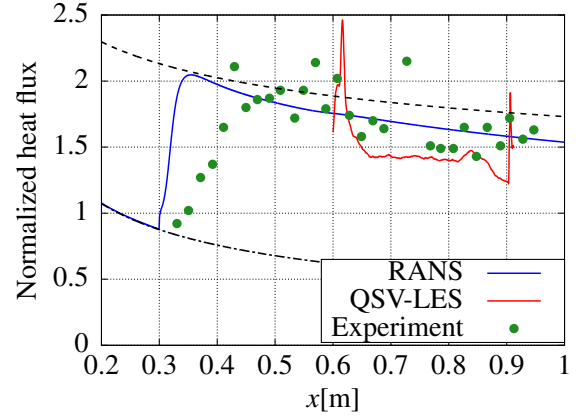


Figure 4. Comparison of wall heat flux profiles between RANS, LES and experiment (Wagner, 2014). The black dashed and dash-dotted lines represent turbulent and laminar heat flux correlations respectively.

collapse on to each other. The agreements of the velocity and temperature implies that the boundary layer does not evolve convolutedly in the present simulation. However, the transformed velocity profile reveals that the data at $x = 0.625$ m deviates from those at the other locations. The deviation at $x = 0.625$ m indicates that self-similarity does not perfectly hold, and the recovery process is not completed at this point. On the other hand, the profiles after $x = 0.7$ m agree well with each other, indicating that the flow field becomes self-similar after this point and therefore the real boundary layer profiles are formed at $x = 0.7$ m and thereafter. This consideration is supported by the velocity fluctuation correlations shown in figure 6. The velocity fluctuation correlations in streamwise and azimuthal directions at $x = 0.625$ m are slightly smaller than the other locations around $y/\delta_{99} = 0.1$. The smaller correlations indicate that turbulence is not fully developed at this point, and this result is consistent with the transformed velocity profiles. In addition, the correlations after $x = 0.7$ m agree well in all directions and thus the boundary layer turbulence is fully developed after $x = 0.7$ m.

Local density fluctuations

To discuss computational FLDI signal, local density fluctuations are extracted from the present LES flow field. Figure 7 shows time history of local density fluctuations at different y locations; $y = 1, 2$ and 3 mm. The density fluctuations are collected at the center in azimuthal direction and at two different x locations; $x = 0.8139$ and 0.8161 m. The distance between

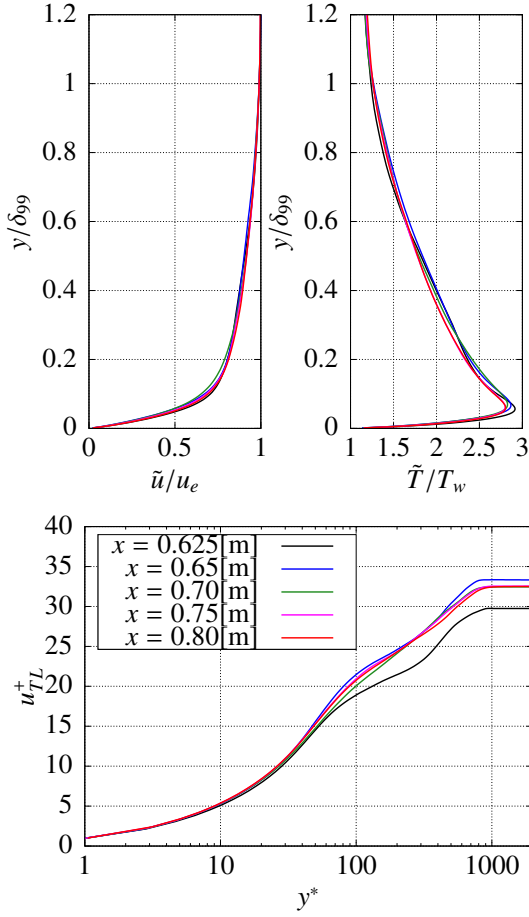


Figure 5. Mean profiles of streamwise velocity (upper left), temperature (upper right) and Streamwise velocity transformed by Trettel & Larsson transformation (Trettel & Larsson, 2016) (bottom).

the two locations is around 2 mm, and this value is comparable with the distance between the two independent FLDI system in the experiment (Camillo & Wagner, 2022).

The comparison of the density fluctuation histories between the two different x -locations shows that their time histories are similar to each other, and the density fluctuation at $x = 0.8161$ m is slightly delayed. This similarity is observed at all y locations. The clear similarity of their time histories indicates that cross-correlations between the different x -locations can provide an accurate estimate of the time lag. Therefore, this result implies that local velocity can be measured by analyzing density fluctuation signals at two different points in experiments.

On the other hand, the comparison of the density fluctuation histories between the different y -locations reveals that density fluctuates more rapidly further away from the wall. To elucidate the reason of the different frequency, instantaneous snapshots of density fluctuations are shown in wall-parallel in figure 8. The density fluctuation at $y = 1$ mm exhibits streaky structures. The structures are long in streamwise direction and the density slightly varies in the streaks. Thus the time scale of the density fluctuation becomes long at $y = 1$ mm. The contour at $y = 2$ mm also has streak structures, but their lengths are shorter than those at $y = 1$ mm. Furthermore, streaky structures no longer exist at $y = 3$ mm, and the density is finely fluctuating in the streamwise direction. Since the time scale of the density fluctuation accompanies the structures of the density

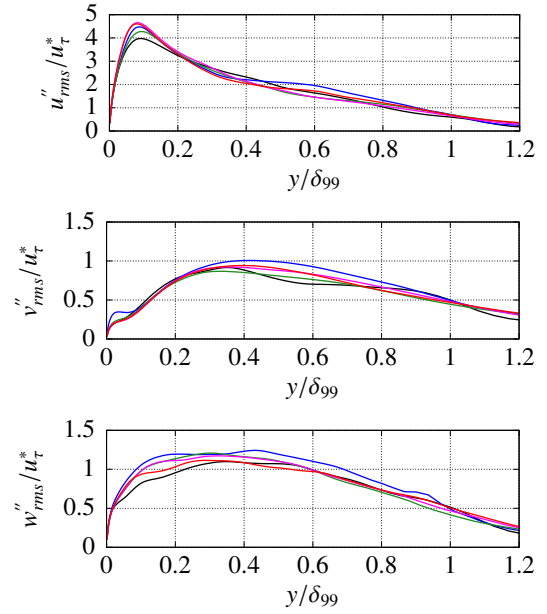


Figure 6. Velocity fluctuation correlations in streamwise (top), wall-normal (middle), and azimuthal directions (bottom). The legend is the same as figure 5.

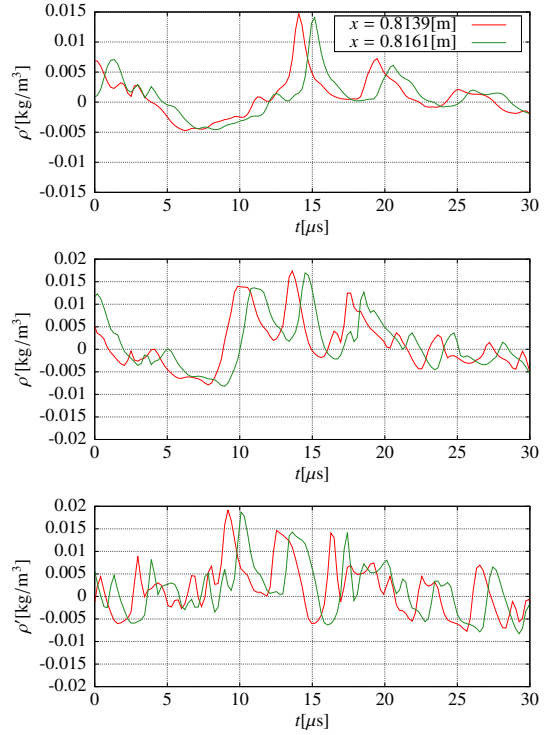


Figure 7. Time history of local density fluctuations at different y locations; $y = 1$ mm (top), $y = 2$ mm (middle), and $y = 3$ mm (bottom).

field, the time scale also becomes shorter further away from the wall.

Conclusion

A large eddy simulation of a hypersonic boundary layer over a 7 degree half angle cone has been performed to compare its results with the FLDI setup described in Camillo & Wag-

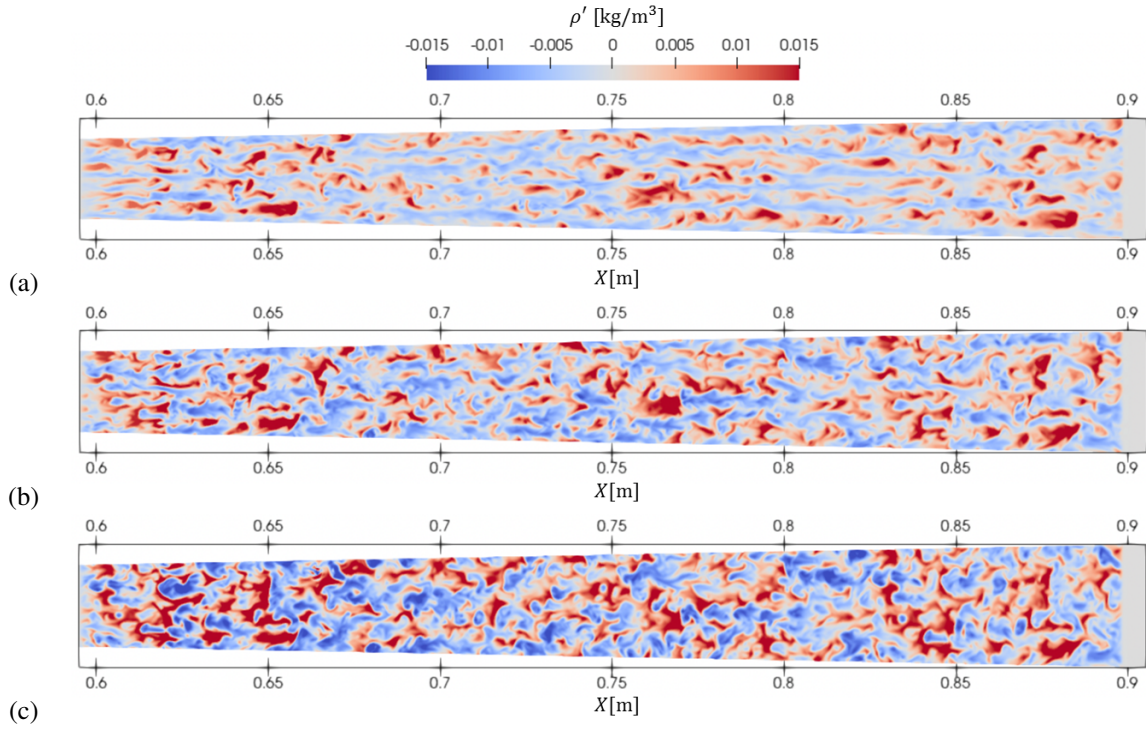


Figure 8. Instantaneous snapshot of density fluctuations in wall parallel planes at $y = 1$ mm (a), 2 mm (b), and 3 mm (c). X denotes a coordinate from the tip of the cone along its axis.

ner (2022). Reynolds number per meter Re_m is $4.1 \times 10^6 \text{m}^{-1}$. To impose reasonable turbulent inlet boundary conditions, the rescaling method described by Urbin & Knight (2001) is used. This paper focuses on computational results in the present LES.

The velocity profiles with the transformation by Trettel & Larsson (2016) and velocity fluctuation correlations become self-similar 0.1 m downstream from the inlet. The measurement point of FLDI in the experiment is located 0.214 m downstream, and thus the self-similarities indicate that real turbulent boundary profiles are formed at the FLDI point.

The time histories of local density fluctuations at two points around 2 mm apart reveal their strong correlations, with the data collected in the downstream side being slightly delayed. This result implies that local velocity can be measured by analyzing cross-correlations between these density fluctuation signals. In addition, The comparison of the time histories between the different y - locations shows that the density fluctuate more rapidly further away from the wall. Examination of wall-parallel planes reveals that the density fluctuate slowly near the wall because the density field has long streaky structures in the streamwise direction. On the other hand, the streaky structures do not persist away from the wall, and the density largely varies in the streamwise direction. The difference of the density flow field induces the different frequency of the density fluctuation. The results of the present QSV-LES will be compared with density fluctuations and convection velocity estimates obtained with the FLDI setup described in Camillo & Wagner (2022) in future research.

REFERENCES

Camillo, Giannino Ponchio & Wagner, Alexander 2022 A low-effort and inexpensive methodology to determine beam separation distance of multi-foci FLDI. *Experiments in Fluids* **63**, 53.

Gottlieb, Sigal 2005 On high order strong stability preserving runge-kutta and multi step time discretizations. *Journal of Scientific Computing* **25**, 105–128.

Hannemann, K., Schramm, J. M., Wagner, A. & Camillo, G. P. 2018 The high enthalpy shock tunnel göttingen of the German Aerospace Center (DLR). *Journal of large-scale research facilities* **4**, A133.

Lawson, J M & Austin, J M 2021 Focused laser differential interferometer response to shock waves. *Measurement Science and Technology* **32** (5), 055203.

Lees, Lester 1956 Laminar heat transfer over blunt-nosed bodies at hypersonic flight speeds. *Journal of Jet Propulsion* **26**, 259–269.

Lele, S. K. 1992 Compact finite difference scheme with spectral-like resolution. *Journal of Computational Physics* **103** (1), 16–42.

Nagarajan, S., Lele, S. & Ferziger, J. 2003 A robust high-order compact method for large eddy simulation. *Journal of Computational Physics* **191**, 392–419.

Parziale, N. J., Shepherd, J. E. & Hornung, H. G. 2012 Differential interferometric measurement of instability in a hypervelocity boundary layer. *AIAA Journal* **51** (3), 750–754.

Sousa, V. C. B., Patel, D., Chapelier, J. B., Wartemann, V., Wagner, A. & Scalò, C. 2019 Numerical investigation of second-mode attenuation over carbon/carbon porous surfaces. *Journal of Spacecraft and Rockets* **56**, 2, 319–332.

Sousa, V. C. B. & Scalò, C. 2022a A unified quasi-spectral viscosity (QSV) approach to shock capturing and large-eddy simulation. *Journal of Computational Physics* **459**, 111139.

Sousa, V. C. B. & Scalò, C. 2022b A Legendre spectral viscosity (LSV) method applied to shock capturing for high-order flux reconstruction schemes. *Journal of Computational Physics* **460**, 111157.

Spalart, P. R. & Allmaras, S. R. 1992 A one-equation turbulence model for aerodynamic flow. *30th aerospace sciences meeting and exhibit pp.* AIAA-92-0439.

Taylor, Geoffrey Ingram & Maccoll, JW 1933 The air pressure on a cone moving at high speeds. -i. *Proceedings of the Royal Society A* **139**, 278–297.

Trettel, A. & Larsson, J. 2016 Mean velocity scaling for compressible wall turbulence with heat transfer. *Physics of Fluids* **28**, 026102.

Urbin, Gerald & Knight, Doyle 2001 Large-eddy simulation

of a supersonic boundary layer using an unstructured grid. *AIAA Journal* **39**, 1288–1295.

Wagner, A. 2014 *Passive Hypersonic Boundary Layer Transition Control Using Ultrasonically Absorptive Carbon-Carbon Ceramic with Random Microstructure*. PhD thesis. Leuven: Katholieke Universiteit.